

Excitonic and impurity-related optical transitions in Be δ -doped GaAs/AlAs multiple quantum wells: Fractional-dimensional space approach

J. Kundrotas, A. Čerškus, S. Ašmontas, and G. Valušis*

Semiconductor Physics Institute, A. Goštauto Street 11, LT-01108 Vilnius, Lithuania

B. Sherliker and M. P. Halsall

School of Electrical and Electronic Engineering, University of Manchester, Manchester M60 1QD, United Kingdom

M. J. Steer

Department of Electronic and Electrical Engineering, University of Sheffield, Sheffield S1 3JD, United Kingdom

E. Johannessen

Microtech Innovation, Ynglingeveien 42, 3184 Borre, Norway

P. Harrison

School of Electronic and Electrical Engineering, University of Leeds, Leeds LS2 9JT, United Kingdom

(Received 17 August 2005; revised manuscript received 21 October 2005; published 19 December 2005)

We have investigated the optical transitions in Be δ -doped GaAs/AlAs multiple quantum wells with various width and doping levels. The fractional dimensionality model was extended to describe free-electron–acceptor (free hole-donor) transitions in a quantum well. The measured photoluminescence spectra from the samples were interpreted within the framework of this model, and acceptor-impurity induced effects in the photoluminescence line shapes from multiple quantum wells of different widths were demonstrated.

DOI: [10.1103/PhysRevB.72.235322](https://doi.org/10.1103/PhysRevB.72.235322)

PACS number(s): 78.55.-m, 78.67.De, 71.30.+h

I. INTRODUCTION

The properties of quantum well (QW) structures are strongly influenced by the presence of doping impurities. The investigation of these impurity effects has both a fundamental interest and is of major importance in device applications such as high electron mobility transistors and QW infrared photodetectors and/or emitters.

Previous works have mainly been focused on barrier-doped (selectively or modulation-doped) structures, whereas the properties of doped QWs, and, in particular, the case for acceptor doping, are less understood. Variations in the properties can be caused by changing the concentration of the dopant from uniform distributions within the QW to concentrated sheet layers resulting in a so-called δ -doped profile. The energetic spectrum of an impurity depends on the width, barrier height, impurity position, and impurity concentration of the QW. Hence, by changing the design of the structure and the doping profile, it is possible to tune in a controlled way the energetic levels. As a general rule, the impurity spectrum lies in the range of several meV. In terms of frequencies, these energies fall into the THz range where the development of compact infrared emitters and small-size detectors is an important issue.^{1–3} Semiconductor QWs are already of great interest for these purposes,^{4–10} and understanding the effect of impurities on the optical properties near the QW intrinsic transitions (such as excitonic transitions) is of particular concern in order to optimize the design of these devices. This is in addition to predicting the infrared emission or absorption spectrum.

The fractional dimensional space (FDS) approach,^{11–13} to our knowledge, was first applied by He (Refs. 14 and 15) to

study optical properties of anisotropic materials. The FDS was found to be a powerful tool in examining the line shape of the interband optical transitions and to elucidate the physical mechanisms defining the anisotropy of the system. The application of this method to the excitonic problem in anisotropic solids enables the calculation of both exciton wave functions and binding energies, as well as the associated optical spectra.¹⁶ The FDS approach can also be used to analyze excitonic features in semiconductor QWs.^{17,18} Further, it can be adapted for magnetic-field-induced effects on shallow-donor states in multiple quantum wells (MQWs)^{19–21} and polaron phenomena in confined systems.^{22,23} However, to our knowledge, it has not been extended to investigate acceptor-impurity-related transitions in semiconductor QWs.

Impurities can be considered as hydrogenlike atoms, and thus the FDS approach can be extended to describe these systems. In that case the discrete bound-state energies and orbital radii for excitons and impurities can be given in Ref. 16:

$$E_n = \frac{Ry}{\left[n + \frac{\alpha - 3}{2} \right]^2}, \quad (1)$$

$$a_n = a_0 \left[n + \frac{\alpha - 3}{2} \right]^2, \quad (2)$$

where $n=1, 2, \dots$ is the principal quantum number, Ry and a_0 denote the Rydberg energy and Bohr radius for exciton or hydrogenlike impurity in the three-dimensional (3D) case, and α labels the dimensionality parameter which changes

from 2 to 3 for idealized QWs. For the 2D case, when $\alpha = 2$, the binding energy of the $1s$ exciton or impurity is a factor of 4 greater than for the 3D case, i.e., $E_1 = 4$ Ry. A more detailed description of the binding energies of the QWs within the FDS approach can be found in Refs. 17–21.

In this work, we have applied the FDS technique for Be acceptor states in GaAs/AlAs MQWs. We have shown that we can describe the excitonic spectra, interband, and Be acceptor related transitions, by the FDS approach and deduce the influence of p -doping effects onto optical properties of QWs having different widths and doping levels.

II. SAMPLES AND EXPERIMENTAL DETAILS

The samples were grown by molecular beam epitaxy on semi-insulating GaAs substrates. The Be δ -doped MQWs contained a different number of wells, $N=200, 50, 40$ with varying well widths L_W of 10, 15, and 20 nm. The AlAs barriers were 5 nm thick in all of the investigated structures. Each of the QW's was δ -doped (2 nm width) with Be acceptors at the center of the well. The doping level for $L_W = 10$ nm MQWs was $5 \times 10^{10} \text{ cm}^{-2}$, $L_W = 15$ nm was $2.5 \times 10^{12} \text{ cm}^{-2}$, while for the MQWs $L_W = 20$ nm two sample doped with 5×10^{10} and $2.5 \times 10^{12} \text{ cm}^{-2}$ were grown.

An argon-ion laser operating in the continuous wave mode was used to excite the photoluminescence (PL). The PL excitation intensity was kept within the range $0.1\text{--}10 \text{ W cm}^{-2}$. The PL signal was dispersed by a monochromator and detected by a cooled photomultiplier operating in a photon counting regime. The PL spectra of the structures were measured at liquid nitrogen (77 K) and room temperatures (300 K).

III. EXPERIMENTAL PHOTOLUMINESCENCE SPECTRA

The PL spectra of the studied MQWs samples at room and nitrogen temperatures are shown in Figs. 1 and 2. A series of clearly resolved peaks can be seen in both figures. The most intensive PL bands are associated with heavy- and light-hole excitonic transitions denoted as X_{e1-hh1} and X_{e1-lh1} , respectively.

In MQWs having widths of $L_W = 15$ and 20 nm, both heavy-hole and light-hole excitonic peaks are almost merged together at room temperature. A closer look at the spectra allows one to discriminate the line E_{e2-hh2} , related to the second sublevel of excited electronic holes (see Fig. 1). The room temperature spectra in the narrowest MQWs, $L_W = 10$ nm, consists of transitions associated with heavy- and light-hole excitons. The arrows (Fig. 1) indicate the calculated value of the sublevel energetic differences of these transitions as described in the figure caption. The parameters used in the calculations are as follows: the conduction-band-energy discontinuity was $Q=0.6$,²⁴ electron effective mass $m_e^*(\Gamma)/m_0=0.0665$,²⁵ valence-band Luttinger parameters $\gamma_1=6.82$, $\gamma_2=2.1$,²⁶ forbidden energy gap $E_g(\Gamma, 300 \text{ K})=1.4256$,²⁷ and for AlAs: $m_e^*(\Gamma)/m_0=0.124$ (Ref. 28) (see comment in Refs. 29 and 30), $\gamma_1=4.04$, $\gamma_2=0.78$ (Ref. 31) (also in Ref. 32), $E_g(\Gamma, 300 \text{ K})=3.02$.³³

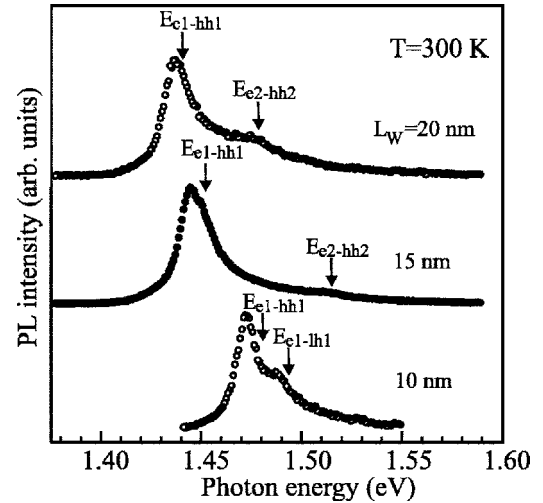


FIG. 1. The PL spectra of the Be δ -doped GaAs/AlAs samples for three different $L_W=10$ nm ($N_{\text{Be}}=5 \times 10^{10} \text{ cm}^{-2}$), 15 nm ($2.5 \times 10^{12} \text{ cm}^{-2}$), and 20 nm ($2.5 \times 10^{12} \text{ cm}^{-2}$) MQWs at room temperature. Arrows indicate E_{e1-hh1} , E_{e2-hh2} , E_{e1-lh1} calculated energy differences from first heavy-hole to first electron, the second heavy-hole to second electron, and the first light-hole to first electron energy levels, respectively. For the sake of clarity, the spectra are shifted vertically.

We observe that at nitrogen (Fig. 2) and room temperatures (Fig. 1), the difference in the energetic position X_{e1-hh1} for $L_W = 10$ nm is $\Delta E = 85.5$ meV. This is in good agreement with the results for GaAs of $\Delta E_g = 86.8$ meV given in Ref. 27. For the other MQWs of $L_W = 15$ and 20 nm, the heavy- and light-hole excitonic peaks are merged at room temperature and comparisons can only be done after deconvolution of the spectra.

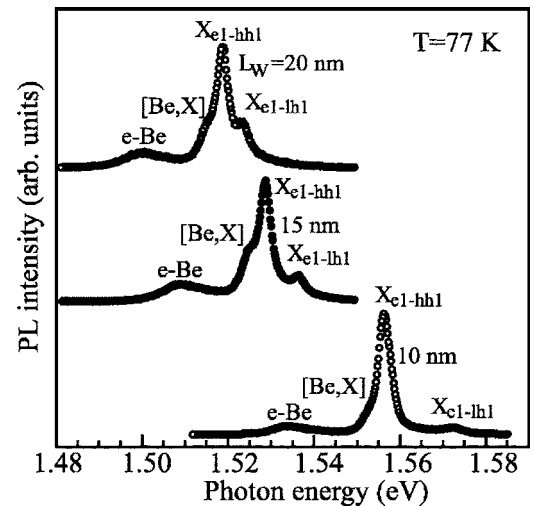


FIG. 2. The PL spectra of Be δ -doped GaAs/AlAs samples with three different $L_W=10$ nm ($N_{\text{Be}}=5 \times 10^{10} \text{ cm}^{-2}$), 15 nm ($2.5 \times 10^{12} \text{ cm}^{-2}$), and 20 nm ($2.5 \times 10^{12} \text{ cm}^{-2}$) MQWs at liquid nitrogen temperature. The symbols X_{e1-hh1} and X_{e1-lh1} indicate heavy-hole and light-hole excitonic transitions, [Be, X]—to Be acceptor-bound exciton, e -Be—free-electron—neutral Be acceptor transitions. For the sake of clarity, the spectra are shifted vertically.

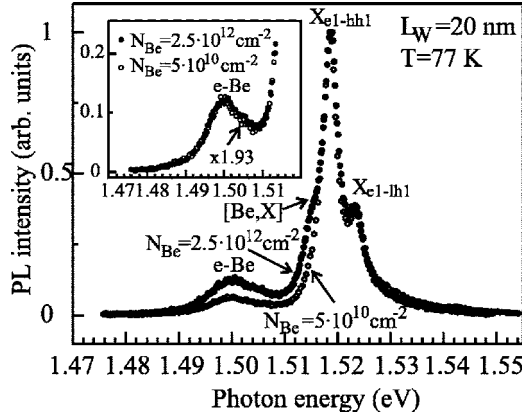


FIG. 3. The PL spectra of the Be δ -doped GaAs/AlAs $L_W = 20$ nm samples for two different $N_{Be} = 5 \times 10^{10} \text{ cm}^{-2}$ (open circles) and $2.5 \times 10^{12} \text{ cm}^{-2}$ (closed circles) MQWs at liquid nitrogen temperature. X_{e1-hh1} and X_{e1-lh1} indicate heavy-hole and light-hole excitonic transitions, [Be, X]—to Be acceptor-bound exciton, e -Be—free-electron-neutral Be acceptor transitions. The inset depicts an enlarged region of the e -Be emission spectra; the weakly doped MQWs PL intensity has been multiplied by a factor of 1.93.

At liquid nitrogen temperatures (Fig. 2), some additional lines appear in the spectrum. The lower energy transitions, labeled as e -Be, are attributed to the recombination of free electrons and holes bound to a Be acceptor. It is also possible to discriminate the line originating from excitons bound to the acceptor impurity, labeled as [Be, X] in the figure.

A knowledge of the transition energies allows a determination of the acceptor binding energy, E_A , using the relation from Ref. 4: $E_A = E(X_{e1-hh1}) + E(X_{hh}) - E(e\text{-Be})$. Here, $E(X_{e1-hh1})$ and $E(e\text{-Be})$ are the energies of the X_{e1-hh1} and e -Be transitions, whereas $E(X_{hh})$ is the binding energy of the heavy-hole exciton which is deduced from theoretical calculations.³⁴ Our estimates show that the acceptor binding energy increases with the decrease of the QW width as predicted in Ref. 8. Considering $L_W = 10$ nm, the acceptor binding energy was found to be $E_A \approx 33$ meV, whereas $E_A \approx 28.5$ meV for a QW with $L_W = 20$ nm. It is worth noting that the obtained values are in good agreement with the estimates given in Ref. 6 at liquid helium temperatures.

It can be seen from Fig. 2 that the excitonic spectra consist of a series of lines labeled on the figure as [Be, X], X_{e1-hh1} , and X_{e1-lh1} . The binding energy of the bound exciton [Be, X] obtained here, $E(X_{e1-hh1}) - E[\text{Be}, X] \approx 3.85$ meV, conforms well with other experimentally findings for GaAs/AlAs (3.7 meV),⁶ and for GaAs/Al_{0.33}Ga_{0.67}As (3.8 meV) (Ref. 35) the QWs, is larger than the value for bulk GaAs $E[A, X] = 2.9$ meV.³⁶

Since the studied MQWs were doped with Be acceptor impurities, it was important to identify the influence of doping in the line shape of the PL spectra. The PL spectra for two MQWs samples at nitrogen temperature are shown in Fig. 3. To display the effects of the doping level we have fitted the e -Be transition in both samples multiplying the weaker spectra by a factor of 1.93. The result is plotted in the inset of Fig. 3. One can clearly see that the line shape is independent of the doping level up to $N_{Be} = 2.5 \times 10^{12} \text{ cm}^{-2}$.

Based on the experimental observations, the sections below are devoted to a more detailed discussion of the spectral features associated with free electrons–Be impurity related transitions. We further extend the model of the FDS to the acceptor states in a QW and apply it to describe the line shape of the free electron–acceptor PL spectrum.

IV. EXCITONIC-RELATED TRANSITIONS

Low-dimensional systems are highly anisotropic. Experimental data obtained, for instance, in semiconductor QWs, are analyzed using isotropic coordinate systems possessing anisotropic Hamiltonians. The excitonic models in these structures usually employ numerical calculations using variational or perturbational approaches. In the idealized case for infinite QWs, the system is presumed to be exactly 2D. However, in real structures (not infinite QWs) excitons or impurities are not 2D anymore. They are in a medium intermediate between 2D and 3D systems since the electron—or hole-wave function penetrates the barrier in the confining dimension. We can therefore consider the structures in another manner, i.e., by applying the approach of fractional dimensions¹¹ and assuming that an anisotropic system in 3D space can be treated as isotropic or unconfined in the effective fractional dimensional space.^{14,15} In this case the single parameter—dimensionality—contains all the information about the anisotropy or confinement of a low-dimensional system. Using this model, He (Ref. 16) has calculated exciton bound-state energies and wave functions of a low-dimensional system by solving the hydrogenic Schrödinger equation in a αD space.

To analyze the excitonic photoluminescence spectra we have used a dimensionless absorption coefficient (optical density), which was theoretically deduced in αD space in Refs. 37 and 38.

$$O(\hbar\omega) = O_0 \left[\sum_{n=1}^{\infty} \frac{4 \text{Ry}_{ex} \Gamma(n + \alpha - 2)}{(n-1)! \left(n + \frac{\alpha-3}{2}\right)^{\alpha+1}} \delta(\hbar\omega - E_n) + \left| \Gamma\left(\frac{\alpha-1}{2} + i\gamma\right) \right|^2 e^{\pi\gamma} \frac{\gamma^{2-\alpha}}{\pi} \Theta(\hbar\omega) \right], \quad (3)$$

$\Theta(\hbar\omega)$ represents the Heaviside step function, $\gamma = \sqrt{\text{Ry}_{ex}/\hbar\omega}$, $\hbar\omega$ is the photon energy, α designates dimensionality, and

$$O_0 = \frac{2^{2\alpha-3} e^2 |d_{cv}|^2 L_c^{\alpha-2} \left[\Gamma\left(\frac{\alpha}{2}\right) \right]^2 \Gamma\left(\frac{\alpha-1}{2}\right)}{\pi^{(\alpha-3)/2} n_B c m_0^2 \omega a_{0ex}^\alpha \text{Ry}_{ex} [\Gamma(\alpha-1)]^3}, \quad (4)$$

where ω is the angular frequency of the incident light, n_B shows the refractive index of the medium, m_0 denotes the free electron mass, e is electronic charge, c stands for the velocity of light, L_c labels the effective length of the active medium, $|d_{cv}|^2$ is the conduction-to-valence squared matrix element of the electron dipole moment, and $\Gamma(x)$ denotes Euler's gamma function.

The absorption coefficient for αD , Eq. (3), is in agreement with well-known results from the literature for 2D and 3D cases.^{39–41} The measurable dimensionless absorption coefficient including Lorentzian line shapes with full width at half maximum w can be calculated from

$$K_{ex} = \int_0^\infty O(\hbar\omega - E) \frac{2w}{\pi(4E^2 + w^2)} dE. \quad (5)$$

The luminescence intensity $I_{PL}(E)$ is related to the absorption coefficient $K(E)$ through the energy balance relation

$$I_{PL}(E) \propto K(E)f(E), \quad (6)$$

where $f(E)$ is a suitable thermal function. In the limit of nondegenerate carrier density, the $f(E)$ can be approximated by a Boltzmann distribution function.

In order to describe the shape of the spectrum it is of particular importance to evaluate the dimensionality parameter α of the confined exciton in the QW. There are several ways to proceed with this problem. For example, in Ref. 17 a simple definition of α on the well width for excitons is proposed:

$$\alpha_{ex} = 3 - \exp\left(-\frac{L_W}{2a_{ex}}\right), \quad (7)$$

where L_W represents the well width and a_{ex} is the exciton effective Bohr radius. This equation is valid for infinite QWs. For real QWs, with finite potential barriers, it can only be used for large QWs comparable to the infinite barrier theoretical device. The microscopic approach for α is proposed in Ref. 18, where one takes into account the penetration of the carriers into the barriers and incorporates the continuous interpolation of the material parameters from their values in the well region to their values in the barrier regions. The second option is to directly calculate the approximate values of α by solving the Schrödinger equation in αD space, as was suggested in Refs. 19–21. However, this method is rather complicated when it comes to interpreting the experimental results, since it requires additional theoretical calculations for all the particular QWs. Therefore, a more convenient way to obtain a dimensionality parameter is to use experimental data or other theoretical methods to calculate values of the exciton binding energies as a function of the well width. The dimensionality can then be determined directly by using Eq. (1).

The absorption coefficients of the interband optical transitions were calculated using the complex dielectric function from Ref. 15:

$$K_{b-b} = \frac{2^{3-\alpha} \pi^{-\alpha/2} e^2 |d_{cv}|^2 L_c^{\alpha-2} \left(\frac{2\mu_{cv}}{\hbar^2}\right)^{\alpha/2}}{\Gamma\left(\frac{\alpha}{2}\right) n_{BC} m_0^2 \omega} \times \sum_\nu (\hbar\omega - E_{QW}^{\nu\nu})^{\alpha/2-1} \Theta(\hbar\omega - E_{QW}^{\nu\nu}), \quad (8)$$

where $\mu_{cv} = m_c^* m_v^* / (m_c^* + m_v^*)$ is the reduced effective mass of the electron and hole. Here $E_{QW}^{\nu\nu}$ is the energy gap between the ν th subband of the conduction, and the ν th subband of the valence band. Equation (8) is in agreement with 2D and

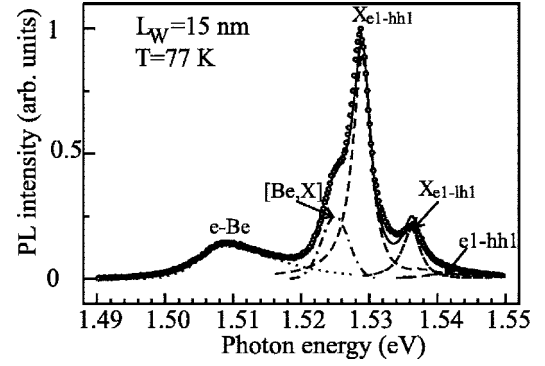


FIG. 4. The PL spectra of the δ -doped GaAs/AlAs MQWs with $L_W = 15$ nm ($N_{Be} = 2.5 \times 10^{12}$ cm $^{-2}$) at liquid nitrogen temperature. X_{e1-hh1} and X_{e1-lh1} indicate heavy-hole and light-hole excitonic transitions, [Be, X] labels exciton bound-to-Be acceptor, e -Be designates electron-neutral Be acceptor transitions, and $e1-hh1$ indicate electron-hole transitions. Dashed lines depict theoretical calculations; solid lines represent the sum of all recombination mechanisms. The dimensionality, full width at half maximum of the Lorentzian or Gaussian convolution (given in parentheses) and relative weightings in the integrated PL spectra for various transitions are as follows: e -Be ($\alpha = 2.87, w_G = 6.4$ meV)–0.23; [Be, X] ($w_G = 4.7$ meV)–0.15; X_{e1-hh1} ($\alpha = 2.3, w_L = 3.5$ meV)–0.5; X_{e1-lh1} ($\alpha = 2.2, w_L = 3.5$ meV)–0.1; $e1-hh1$ ($\alpha = 2.3, w_L = 3.5$ meV)–0.02.

3D cases^{41,42} and the band-band transitions of the Lorentzian convolution [see Eq. (5)] was also included for clarity.

The calculations for $L_W = 15$ nm ($N_{Be} = 2.5 \times 10^{12}$ cm $^{-2}$) of each transition observed in the PL spectrum together with the experimental data at liquid nitrogen temperature is presented in Fig. 4. The excitonic PL spectra and interband transitions were calculated by the FDS approach including Lorentzian convolution, whereas the line shape of bound excitons [Be, X] was approximated by a Gaussian. The dimensionality was extracted using Eq. (1) from the exciton binding energy calculated in Ref. 34 and $Ry_{ex} = 4.2$ meV.⁴³ For the interband transitions, only the transitions of $e1-hh1$ from the first electron to heavy-hole sublevel were included. It is clear that the chosen model provides a good description of the overall PL spectrum at liquid nitrogen temperature. It can be inferred that at liquid nitrogen temperatures, the near edge PL region is dominated by excitonic related optical transitions. The interband transitions are negligible and amount to a only a few percent of the total PL intensity. More details about the e -Be transitions will be presented in Sec. V.

The calculated results at room temperature for $L_W = 10$ nm and $L_W = 15$ nm are shown in Figs. 5 and 6. For the analysis of the spectrum of the QW with width $L_W = 10$ nm, we have included heavy-hole, light-hole excitonic, and interband $e1-hh1$ transitions. For the QW with $L_W = 15$ nm, we have also taken into account the second sublevel system. The peak observed in Fig. 6 for $L_W = 15$ nm at a photon energy of $\hbar\omega = 1.51$ eV, is attributed to the transitions from $e2$ to $hh2$ according to the selection rules. In this transition, the excitonic effects were also taken into account. More specifically, in the infinite-rectangular-well approximation, due to the orthogonality of the envelope wave function, only transitions between confined valence and conduction states with the

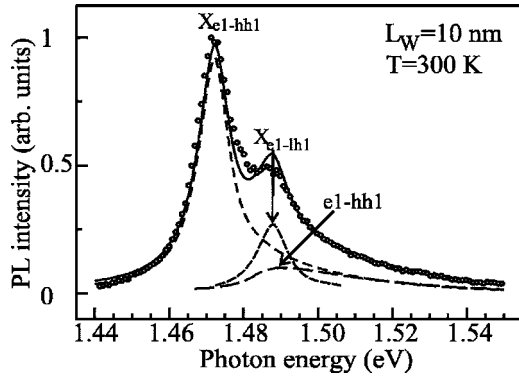


FIG. 5. The PL spectra of the Be δ -doped GaAs/AlAs $L_w = 10$ nm MQWs at room temperature. Symbols X_{e1-hh1} and X_{e1-lh1} indicate heavy-hole and light-hole excitonic transitions and $e1-hh1$ depict electron-hole transitions. Dashed lines are the theory, the solid line shows the sum of both excitonic and $e1-hh1$ transitions. The dimensionality (given in parentheses) and relative weightings in the integrated PL spectra for various transitions are as follows: X_{e1-hh1} ($\alpha=2.2$)-0.66; X_{e1-lh1} ($\alpha=2.06$)-0.17; $e1-hh1$ ($\alpha=2.2$)-0.12. For all the peaks the full width at half maximum of the Lorentzian convolution was found to be $w_L=11$ meV.

same quantum number are allowed.^{44,45} These transitions are strongest in the absorption, PL, and PL excitation spectra^{46,47} of QW systems. The exciton binding energies for higher levels are lower compared to the first sublevels, but the difference is small.^{48,49} It should be noted that the higher electron states correspond to wave functions which penetrate more into the barriers, and thus the overlap with the hole wave function is smaller. However, this effect is compensated if conduction-band nonparabolicity is included.⁵⁰ In the following calculations we take the exciton binding energy associ-

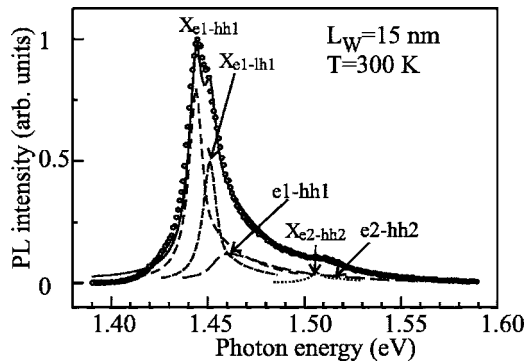


FIG. 6. The PL spectra of the Be δ -doped GaAs/AlAs $L_w = 15$ nm MQWs at room temperature. Symbols X_{e1-hh1} , X_{e2-hh2} , and X_{e1-lh1} indicate heavy-hole and light-hole excitonic transitions. Dashed lines are the theory, solid lines represent the sum of excitonic and both $e1-hh1$, $e2-hh2$ transitions. The dimensionality (given in parentheses) and relative weightings in the integrated PL spectra for various transitions are as follows: X_{e1-hh1} ($\alpha=2.3$)-0.49; X_{e1-lh1} ($\alpha=2.2$)-0.27; X_{e2-hh2} ($\alpha=2.5$)-0.03; $e1-hh1$ ($\alpha=2.3$), and $e2-hh2$ ($\alpha=2.5$)-0.21. For all curves the full width at half maximum of the Lorentzian convolution was found to be $w_L=9$ meV.

ated with the excited levels to be equal to $E(X_{e2-hh2}) = 7.5$ meV which corresponds to the dimensionality of $\alpha = 2.5$.

The next important feature of spectra is the doublet structure of the $e2-hh2$ transition.^{46,47} This splitting is a result of the heavy and light exciton mixing.⁴⁷ In our experiments this delicate effect is not observed and therefore is not included into the calculations. The nonparabolicity of interband $e2-hh2$ transitions⁵¹⁻⁵⁴ was taken into account, but its contribution in our PL spectra is negligible. However, nonparabolicity is more important in the evaluation of the actual transition energy. The results of the calculations concerning the contribution of the excited sublevels are given in Fig. 6. Symbol X_{e2-hh2} indicates heavy hole while $e2-hh2$ shows excited band-to-band transitions.

The analysis shows that excitons are important at high temperatures (up to room temperature) not only in the absorption spectra,⁵⁵ but also in the PL spectra. The GaAs/AlAs MQWs interband transitions add up to one-fifth of the integrated PL intensity at room temperature, whereas the rest is related to the excitonic transitions. The opposite is generally the case in pure GaAs.⁵⁶

In the modeling of the line shape, we have assumed that the broadening of the excitonic PL linewidth consists of two components: a homogeneous and an inhomogeneous part:⁵⁷

$$\Gamma = \Gamma_0 + aT + b/[\exp(\hbar\omega_{LO}/kT) - 1], \quad (9)$$

where Γ_0 is the temperature T independent inhomogeneous width, while the second and third terms arise from the increase of the exciton scattering by acoustic and optical phonons with temperature, respectively. Coefficients a and b represent corresponding scattering strengths. As a general rule, the Γ value is obtained from the measured PL spectra using Gaussian or Lorentzian convolution procedures.

It is expected that at very low temperatures when the exciton-phonon scattering is inefficient, the exciton PL spectra are inhomogeneously broadened, and Gaussian convolution should be used. The line shape becomes closer to a Lorentzian at higher temperatures.⁵⁸⁻⁶¹

The exciton-acoustic-phonon interaction coefficient is generally in the range $a \approx 2-10 \mu\text{eV K}^{-1}$,⁶²⁻⁶⁶ and the exciton-LO-phonon interaction coefficient in the range $b \approx 10-15$ meV.^{64,66} The values obtained for our samples are the following: $\Gamma_0 \approx 2.5$ meV, $\Gamma(T=77 \text{ K}) \approx 3.5$ meV, and $\Gamma(T=300 \text{ K}) \approx 9-11$ meV. These values correspond to coefficients for acoustic scattering $a \approx 12 \mu\text{eV K}^{-1}$ and optical scattering, $b \approx 8.4-14.8$ meV, respectively. These data conform well to both the results presented by the authors cited above and the theoretical predictions. One must note, however, that in the case when the lines of heavy- and light-hole excitons are merged at 300 K, the excitonic PL band is twice as wide in comparison to separated bands. This can be seen by comparing the results for $L_w=15$ and 20 nm with that for $L_w=10$ nm at 300 K in Fig. 1 or by comparing the results in Figs. 5 and 6.

V. IMPURITY-RELATED TRANSITIONS

Understanding the effect of impurities is of fundamental importance in order to determine the electronic, optical, and

transport properties of QWs. Most of these properties depend on the doping level of the impurity. Properties of weakly doped QWs can be explained by a model assuming noninteracting impurities. However, as the impurity concentration increases, one reaches a situation where the single-impurity theory is no longer valid. This effect is caused by the overlap of the impurity wave functions becoming significant. At this concentration the formation of the impurity band starts causing tails to form at the edge of the first conduction or valence subband edge which is dependent on the doping type, n type or p type. Very high dopant concentration causes an overlap of the impurity band with the free-carrier continuum. This threshold corresponds to the transition from insulating to metallic behavior of the carriers (the Mott transition). In the high-density limit of δ -doped semiconductors and QWs, the electrons (holes) are confined to the ionized sheets of the impurities and form a two-dimensional electron (hole) gas with a two-dimensional subband structure.

In QWs the impurity binding energy becomes larger than in the 3D case, whereas the effective Bohr radius decreases. This means that critical concentrations to form the impurity band and to create the Mott transition are higher than in the 3D case where the criterion of Mott transitions is the constant value of products of the cube root of the impurity density and Bohr radius.⁶⁷ For example, our estimates show that the critical concentration for an insulator-metal transition and the formation of subband structure with Be δ -doped GaAs/AlAs QWs $L_W=5$ nm occurs at acceptor concentration near or greater than $N_{Be} > 5 \times 10^{12} \text{ cm}^{-2}$.⁶⁸

As shown in Fig. 3, the e -Be transitions line shape is independent of impurity concentration up to $N_{Be}=2.5 \times 10^{12} \text{ cm}^{-2}$ and this line is not merged with the excitonic PL region. It means that no formation of an impurity band occurs under these conditions. Consequently, we can analyze impurity-related transitions for noninteracting impurities. It is worth noting that the FDS approach may be adapted for impurities if they are fixed in a δ -doped sheet in the well, since the impurity energy spectrum depends on the position in the QW. If impurities are homogeneously distributed in the QW, the task becomes more complicated as it requires finding a dimensionality α for all the positions within the well.^{20,21}

In our studies we have assumed that the acceptor impurities are in the center of the QW and that their energy and transition probabilities are independent of the location in the QW. Also, we took into account the valence-band structure of the acceptor presuming that the inclusion of the heavy-hole state is completely sufficient to describe spectral features.⁶⁹ Further, in our approximations, the Bloch functions for electrons and acceptor impurities in the QW are considered to be isotropic. Since the quantum well widths used here are large in comparison to the lattice constant of the bulk semiconductor, it is reasonable to suppose that the quantum confinement modifies only the plane-wave envelope part of the wave functions, and does not change the lattice-periodic part function.⁴¹ Taking these assumptions into account, the envelope wave function for free electrons and acceptors can be considered in the FDS space, where only the dimension determines the degree of anisotropy or confinement. In this case, the absorption coefficient of the

acceptor-conduction-band (first electron energy level) transitions can be calculated using Eagles'⁷⁰ or Dumke's⁷¹ approach.⁷²

In fact, to define absorption coefficients in low-dimensional structures is complicated, and this issue is already discussed in Refs. 37, 41, 45, and 73. Following the ideology of Lefebvre,³⁷ we have calculated the dimensionless absorption coefficient. Initially, the probability for photon absorption has to be considered within the dipole approximation neglecting the photon wave vector which involves the conduction band and shallow acceptor⁷⁴:

$$W_{if} = \frac{2\pi}{\hbar} |d_{cv}|^2 |a(k)|^2 \rho(k) \delta(\hbar\omega - E_{QW} + E_A), \quad (10)$$

where $|d_{cv}|^2$ is the conduction-to-valence squared matrix element of the electron dipole moment, $\rho(k)$ is a product of final and initial number of states, E_{QW} is the energy difference from hole to electron levels in a QW, and E_A the acceptor binding energy. The absorption coefficient for the acceptor free electron transition obeys the relation

$$K = \frac{4\pi^2 e^2}{n_B c m_0^2 \omega S} |d_{cv}|^2 |a(k)|^2 \rho(E), \quad (11)$$

where the energy $E = \hbar\omega - E_{QW} + E_A$, and $\rho(E)$ (which, for example, in the 3D case⁷⁵) can be assumed as

$$\rho(E) = g_I N_I S G_\alpha(\hbar\omega), \quad (12)$$

where g_I is the impurity level degeneracy, N_I is the impurity concentration in $[1/\text{cm}^2]$. The term $G_\alpha(E)$ represents the density of states in the FDS approach and is expressed in Ref. 14:

$$G_\alpha(E) = \frac{2V_\alpha}{\Gamma\left(\frac{\alpha}{2}\right)} \left(\frac{m_c^*}{2\pi\hbar^2}\right)^{\alpha/2} E^{\alpha/2-1} \Theta(E), \quad (13)$$

where $\Theta(E)$ is the Heaviside step function, and term 2 takes into account the spin degeneracy. The term V_α is the volume in a αD space, which is given by the Hausdorff measure:

$$V_\alpha(r) = \frac{\pi^{\alpha/2}}{\Gamma\left(1 + \frac{\alpha}{2}\right)} r^\alpha. \quad (14)$$

For a hydrogenlike approximation of the acceptor impurity and simple valence-band structures, shallow acceptor wave functions can be expanded as a linear combination of valence-band functions and the motion of free carriers. These can be described by a plane-wave function in the FDS,¹¹ and leads to the result that $a(\mathbf{k})$ is a Fourier transformation of an acceptor hydrogenlike function:⁷²

$$a(k) = \int e^{-i\mathbf{k}\mathbf{r}} F(\mathbf{r}) d\mathbf{r}, \quad (15)$$

where $F(\mathbf{r})$ is the acceptor hydrogenlike function in FDS:¹⁶

$$F(r) = \left[\frac{2^{\alpha+1} \pi^{(1-\alpha)/2}}{\Gamma\left(\frac{\alpha-1}{2}\right) (\alpha-1)^{\alpha+1} a_B^\alpha} \frac{1}{e^{-2/(\alpha-1)(r/a_B)}} \right]^{1/2}, \quad (16)$$

where a_B is the acceptor Bohr radius in the 3D case. The Fourier transformation in FDS reads¹¹

$$a(k) = (2\pi)^{\alpha/2} \int_0^\infty r^{\alpha-1} (kr)^{1-\alpha/2} J_{\alpha/2-1}(kr) F(r) dr, \quad (17)$$

where $J_{\alpha/2-1}(kr)$ represents the Bessel function. The coefficient squared $|a(\mathbf{k})|^2$ in FDS is given by

$$|a(\mathbf{k})|^2 = 2^\alpha \pi^{(\alpha-1)/2} (\alpha-1)^\alpha \Gamma\left(\frac{1+\alpha}{2}\right) \frac{a_B^\alpha}{V_\alpha \left[1 + a_B^2 k^2 \left(\frac{\alpha-1}{2}\right)^2 \right]^{1+\alpha}}. \quad (18)$$

From this approximation following some algebraic manipulations, we obtain

$$K = N_I g_I \frac{4\pi^2 e^2}{cn_B m_0^2 \omega} |d_{cv}|^2 \frac{2^{\alpha+1} \Gamma\left(\frac{\alpha+1}{2}\right) \left(\frac{m_c^*}{m_p^*}\right)}{\pi^{1/2} \Gamma\left(\frac{\alpha}{2}\right) \text{Ry}_I \left(\frac{2}{\alpha-1}\right)^2} \frac{1}{\left[1 + \frac{m_c^*}{m_p^*} \frac{E}{\text{Ry}_I \left(\frac{2}{\alpha-1}\right)^2} \right]^{\alpha+1}} \left[\frac{m_c^*}{m_p^*} \frac{E}{\text{Ry}_I \left(\frac{2}{\alpha-1}\right)^2} \right]^{\alpha/2-1} \Theta(E), \quad (19)$$

where Ry_I is the acceptor binding energy in the 3D case. The acceptor binding energy in αD space from Eq. (1) for $n=1$ is equal:

$$E_A = \text{Ry}_I \left(\frac{2}{\alpha-1}\right)^2. \quad (20)$$

The absorption coefficient [Eq. (19)] can be adapted for donor-to-valence-band transitions by replacing the effective masses and acceptor binding energy instead of the donor binding energy.⁷¹

In the 3D case, the absorption coefficient for the acceptor free electron transition obeys

$$K = N_I \frac{128\pi g_I e^2}{cn_B m_0^2 \omega} |d_{cv}|^2 \left(\frac{m_c^*}{m_p^*}\right) \frac{1}{E_A} \frac{x^{1/2}}{[1+x]^4}, \quad (21)$$

where

$$x = \left(\frac{m_c^*}{m_p^*}\right) \frac{E}{\text{Ry}_I \left(\frac{2}{\alpha-1}\right)^2} = \left(\frac{m_c^*}{m_p^*}\right) \frac{E}{E_A}. \quad (22)$$

Taking $g_I=2$ for donors, or $g_I=4$ for acceptors, respectively, N_I in $[1/\text{cm}^3]$, we obtain absorption coefficients that consists with well-known results from literature.^{70,71} For the 2D case, the expression can be written as

$$K = N_I \frac{16\pi^2 g_I e^2}{cn_B m_0^2 \omega} |d_{cv}|^2 \left(\frac{m_c^*}{m_p^*}\right) \frac{1}{E_A} \frac{\Theta(x)}{[1+x]^3}. \quad (23)$$

In this case $E_A=4 \text{ Ry}_I$ and the absorption coefficients are in agreement with the calculations from Ref. 76.

As mentioned previously, impurities in a QW can be distributed either homogeneously or being δ -doped. In the case of a homogeneous distribution, the impurity energy depends on its location within the QW, and the analysis of free electron transitions with acceptors (or free holes with donors) is complicated. As a general rule in this case, one can observe an experimentally obtained double-peak structure in the free-electron-acceptor transitions.^{4,77} This double peak structure is attributed to the recombination of free electrons with acceptors at the QWs center and interface, and is of qualitative agreement with the theoretical calculations.^{76,78} However, by comparison between the experimental and calculated electron-to-acceptor PL line shapes of nominally undoped GaAs/Al_xGa_{1-x}As QWs,⁷⁹ the authors claimed that the acceptor distribution exhibited a maximum at the well interface, extending 0.7 nm into the barrier and 1.2 to 3 nm into the well. Similar spectra were calculated theoretically in Ref. 78. However, a similar line shape requires the assignment of a quasi-Fermi-energy level for the electron gas. The doublet nature of the free heavy hole-to-donor line in GaAs/Al_xGa_{1-x}As QWs was also observed.⁸⁰ In this case, the authors explained that this doublet corresponded to a

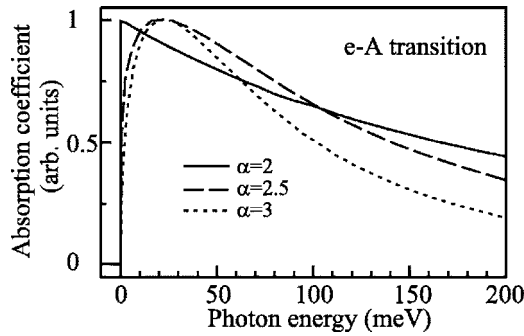


FIG. 7. The spectral shape of the electron-acceptor transition absorption coefficient. The quantum well dimensionality is given as a parameter. The energetic scale is relative and shifted by the forbidden quantum well energy minus the acceptor binding energy for all of the dimensionality cases.

monolayer variation in the well size. The experiments and theoretical considerations from the literature show that a complete understanding of the free carriers to impurity recombination in QWs remains open and requires a direct comparison between experimental and theoretical results.

In our experimental and theoretical considerations, we have assumed that the impurities are concentrated in the sheet and fill only a small part of the QW. Therefore, it does not require a weighting of the recombination process over the well width and we can directly apply the theoretical approach given above.

We have calculated the free-electron-acceptor absorption coefficient from Eq. (19) and the PL line shape from Eq. (6) for the GaAs/AlAs QW with varying dimensionality parameters. In the calculations we used $Ry_{Be}=28$ meV (Ref. 81) and $m_c^*/m_p^*=0.17$. The calculated results are presented in Figs. 7 and 8. One can see that owing to the small ratio m_c^*/m_p^* , the absorption coefficient represents a slowly decreasing function of energy above the threshold. However, the PL line shape from the higher energy side is resolved by a thermal distribution function. From the analysis of PL curves we can conclude that the PL line shape is asymmetrical and cannot be described directly, for example, as a

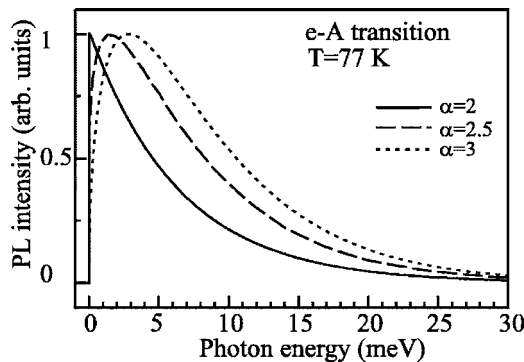


FIG. 8. The calculated line shape of the free-electron-acceptor photoluminescence intensity on the QW dimensionality at liquid nitrogen temperature. The energetic scale is relative and shifted by the forbidden QW energy minus acceptor binding energy for all the dimensionality cases.

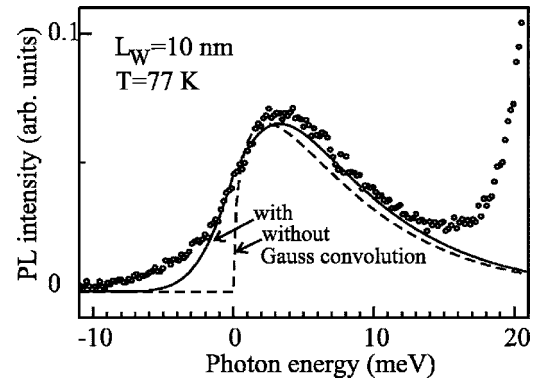


FIG. 9. The spectral shape of the free-electron-acceptor transition in $L_W=10$ nm width MQWs ($N_{Be}=5 \times 10^{10}$ cm $^{-2}$) at liquid nitrogen temperature. Points show experimental data, lines denote theory: the dotted line is without and solid line is with the Gaussian convolution; the full width at half maximum is $w_G=6$ meV. Dimensionality $\alpha=2.8$. The energetic scale is relatively and shifted by the forbidden quantum well energy minus the acceptor binding energy.

Gaussian-type function. It can be noted that for the valence-band-donor transitions, the ratio of effective masses m_p^*/m_c^* is sufficiently large for the absorption coefficient (in contrast to the case for free-electron-acceptor transitions) to become a fairly rapidly decreasing function of energy above the threshold.

To describe the spectral shape of the observed free-electron-to-acceptor transition, we applied a Gaussian convolution in order to obtain a realistic fractional-dimensionality calculation which includes random distribution of impurities in their sheet. The modeling results and the experimental data for the QW of 15 and 10 nm width at 77 K are presented in Figs. 4 and 9, respectively. It is clear that the use of a Gaussian convolution parameter with full width at half maximum $w_G=6.4$ meV for $L_W=15$ nm and $w_G=6$ meV for $L_W=10$ nm, provides an excellent agreement with the experimental results. In contrast, without the Gaussian convolution one can only approximate the high energy wing of the spectrum, while the low energy part in the simulations remains “steplike” (see Fig. 9), and hence does not fit into the experimental data. Knowing that dopants cause band edge fluctuations—so-called random potential or disorder—this effect, together with the phonon interaction, affects PL spectra inducing broadening in free-electron-to-acceptor PL line shape.^{82,83} The dimensionality was estimated from experimental acceptor binding energy, using Eq. (20). Note that the line shape of the transition is asymmetric. We suppose that this PL spectral feature is defined mainly by the spectral shape of the absorption coefficient and its product with carrier distribution function. The influence of energetically higher lying Γ_7 light-hole acceptor states on the PL spectral shape should be negligible⁸⁴ because its splitting from between heavy-hole states amounts only from 0.55 up to 0.65 meV if the QW width decreases from 15 to 10 nm.⁸⁵

Finally, we will briefly comment on the influence of electron-phonon interactions on the threshold energy of the free-electron-acceptor transition. We believe that the threshold energy and the acceptor binding energy are two different parameters. In Fig. 8, we can conclude that the maximum of

free-electron–acceptor spectra is blueshifted by a few meV from the threshold energy. However, we have ignored the electron-phonon interaction in our calculations which exhibit a strong effect in polar materials such as GaAs. These interactions are known to cause longitudinal optical phonon sidebands which have been observed for the free-electron–acceptor transitions in GaAs (Ref. 86) and GaAs/AlAs MQWs.⁸⁷ The LO-phonon interaction causes a redshift of the threshold energy,⁸⁸ whose value is a few meV, and there was an observed discrepancy between the threshold energy and acceptor binding energy in our experiments. This is the reason why, in order to overcome this effect, the true free-electron–acceptor transition energy should be interpreted close to the maximum of the PL spectra.

Our experimental results and theoretical calculation are in excellent agreement with previous studies of the 3D case.⁸⁹ One can clearly see that the FDS approach can be successfully used to analyze free-electron–acceptor impurities located in all positions of the QWs. The only condition that implies the impurities should be located in a sheet, and that their concentration should be low enough to provide no interaction between them. In this case our model can successfully be used to analyze free holes-to-donors transitions in QWs.

VI. CONCLUSIONS

We have examined both, experimentally and theoretically, the photoluminescence spectra of the Be δ -doped GaAs/AlAs QWs with different widths of 10, 15, and 20 nm, combined with various doping levels ranging from $5 \times 10^{10} \text{ cm}^{-2}$ to $2.5 \times 10^{12} \text{ cm}^{-2}$. We have analyzed intrinsic

PL spectra using the fractional dimensional approach and estimated contributions of the excitonic and interband transitions to the photoluminescence spectra at liquid nitrogen and room temperatures. It was determined that at 77 K excitonic-related optical transitions predominate whereas interband transitions' part is negligible and amounts only up to a few percent. The analysis at 300 K has shown that excitons are important at high temperatures (up to room temperature) in the photoluminescence spectra. The interband transitions add up to one-fifth of the integrated photoluminescence intensity, whereas the remainder part is assigned to be related to the excitonic transitions. We have extended the fractional-dimensional approach to analyze transitions of the free-electron–acceptor impurities located in the center of the quantum well. By applying this theoretical model we have explained the photoluminescence line shape for different quantum wells. An applied approach with inclusion of the Gaussian convolution was able to describe excellently the obtained experimental data.

ACKNOWLEDGMENTS

The collaboration between the Semiconductor Physics Institute at Vilnius and Universities of Leeds, Manchester, and Sheffield was supported, in part, by the project Centre of Processing, Research and Application of Advanced Materials (PRAMA) from the European Commission by the Programme Centres of Excellence and Lithuanian State Science and Studies Foundation (Project No. T-06086). The research conducted in the Semiconductor Physics Institute at Vilnius was performed under the topic “Study of semiconductor nanostructures for terahertz technologies” (No. 144.1).

*Corresponding author. Electronic address: valusis@pfi.lt

¹F. Szmulowicz, T. Oogarah, J. Ehret, K. Mahalingam, H. C. Liu, S. M. Hegde, J. Solomon, D. Tomich, G. Landis, and G. J. Brown, *Phys. Rev. B* **68**, 085305 (2003).
²B. F. Levine, *J. Appl. Phys.* **74**, R1 (1993).
³H. C. Liu, C. Y. Song, A. J. SpringThorpe, and J. C. Cao, *Appl. Phys. Lett.* **84**, 4068 (2004).
⁴R. C. Miller, A. C. Gossard, W. T. Tsang, and O. Munteanu, *Phys. Rev. B* **25**, 3871 (1982).
⁵Q. X. Zhao, S. Wongmanerod, M. Willander, P. O. Holtz, S. M. Wang, and M. Sadeghi, *Phys. Rev. B* **63**, 195317 (2001).
⁶W. M. Zheng, M. P. Halsall, P. Harmer, P. Harrison, and M. J. Steer, *J. Appl. Phys.* **92**, 6039 (2002).
⁷W. M. Zheng, M. P. Halsall, P. Harmer, P. Harrison, and M. J. Steer, *Appl. Phys. Lett.* **84**, 735 (2004).
⁸W. T. Masselink, Yia-Chung Chang, and H. Morkoç, *Phys. Rev. B* **32**, 5190 (1985).
⁹C. Mailhiot, Yia-Chung Chang, and T. C. McGill, *Phys. Rev. B* **26**, 4449 (1982).
¹⁰X. Liu, A. Petrou, B. D. McCombe, J. Ralston, and G. Wicks, *Phys. Rev. B* **38**, R8522 (1988).
¹¹F. H. Stillinger, *J. Math. Phys.* **18**, 1224 (1977).
¹²Z. Bak, *Phys. Rev. B* **68**, 064511 (2003).

¹³C. Palmer and P. N. Stavrinou, *J. Phys. A* **37**, 6987 (2004).

¹⁴X. F. He, *Solid State Commun.* **75**, 111 (1990).

¹⁵X. F. He, *Phys. Rev. B* **42**, 11751 (1990).

¹⁶X. F. He, *Phys. Rev. B* **43**, 2063 (1991).

¹⁷H. Mathieu, P. Lefebvre, and P. Christol, *Phys. Rev. B* **46**, 4092 (1992).

¹⁸P. Christol, P. Lefebvre, and H. Mathieu, *J. Appl. Phys.* **74**, 5626 (1993).

¹⁹A. Matos-Abiague, L. E. Oliveira, and M. de Dios-Leyva, *Phys. Rev. B* **58**, 4072 (1998).

²⁰M. de Dios-Leyva, A. Bruno-Alfonso, A. Matos-Abiague, and L. E. Oliveira, *J. Phys.: Condens. Matter* **9**, 8477 (1997).

²¹E. Reyes-Gómez, A. Matos-Abiague, C. A. Perdomo-Leiva, M. de Dios-Leyva, and L. E. Oliveira, *Phys. Rev. B* **61**, 13104 (2000).

²²A. Matos-Abiague, *Phys. Rev. B* **65**, 165321 (2002).

²³A. Thilagam and A. Matos-Abiague, *J. Phys.: Condens. Matter* **16**, 3981 (2004).

²⁴R. C. Miller, D. A. Kleinman, and A. C. Gossard, *Phys. Rev. B* **29**, R7085 (1984).

²⁵G. E. Stillman, C. M. Wolfe, and J. O. Dimmock, *Solid State Commun.* **7**, 921 (1969).

²⁶K. Hess, D. Bimberg, N. O. Lipari, J. U. Fischbach, and M. Al-

- tarelli, in *Proceedings of the 13th International Conference on the Physics of Semiconductors, Rome, 1976*, edited by F. G. Fumi (Rome, 1976), p. 142.
- ²⁷G. Oelgart, B. Orschel, M. Proctor, D. Martin, F. Morier-Genoud, and F. K. Reinhart, *J. Appl. Phys.* **74**, 2742 (1993).
- ²⁸W. P. Dumke, M. R. Lorenz, and G. D. Pettit, *Phys. Rev. B* **5**, 2978 (1972).
- ²⁹V. Fiorentini and A. Baldereschi, *J. Phys.: Condens. Matter* **4**, 5967 (1992).
- ³⁰V. Fiorentini, *Phys. Rev. B* **46**, 2086 (1992).
- ³¹P. Lawaetz, *Phys. Rev. B* **4**, 3460 (1971).
- ³²L. Pavesi and M. Guzzi, *J. Appl. Phys.* **75**, 4779 (1994).
- ³³M. Garriga, P. Lautenschlager, M. Cardona, and K. Ploog, *Solid State Commun.* **61**, 157 (1987).
- ³⁴L. C. Andreani and A. Pasquarello, *Phys. Rev. B* **42**, 8928 (1990).
- ³⁵D. Boffety, A. Vasson, A.-M. Vasson, J. Leymarie, T. S. Cheng, C. A. Bates, and J. M. Chamberlain, *Semicond. Sci. Technol.* **11**, 340 (1996).
- ³⁶W. Bludau and E. Wagner, *Phys. Rev. B* **13**, 5410 (1976).
- ³⁷P. Lefebvre, P. Christol, and H. Mathieu, *Phys. Rev. B* **48**, 17308 (1993).
- ³⁸P. Lefebvre, P. Christol, and H. Mathieu, *Superlattices Microstruct.* **17**, 19 (1995).
- ³⁹R. J. Elliott, *Phys. Rev.* **108**, 1384 (1957).
- ⁴⁰M. Shinada and S. Sugano, *J. Phys. Soc. Jpn.* **21**, 1936 (1966).
- ⁴¹H. Haug and S. W. Koch, *Quantum Theory of the Optical and Electronic Properties of Semiconductors* (World Scientific, Singapore, 1990).
- ⁴²E. L. Ivchenko and G. E. Pikus, *Superlattices and Other Heterostructures. Symmetry and Optical Phenomena* (Springer-Verlag, Berlin-Heldelberg, 1997).
- ⁴³S. B. Nam, D. C. Reynolds, C. W. Litton, R. J. Almassy, T. C. Collins, and C. M. Wolfe, *Phys. Rev. B* **13**, 761 (1976).
- ⁴⁴R. Dingle, W. Wiegmann, and C. H. Henry, *Phys. Rev. Lett.* **33**, 827 (1974).
- ⁴⁵G. Bastard, *Wave Mechanics Applied to Semiconductor Heterostructures* (Les Editions de Physique, Paris, 1988).
- ⁴⁶R. C. Miller, A. C. Gossard, G. D. Sanders, Yia-Chung Chang, and J. N. Schulman, *Phys. Rev. B* **32**, R8452 (1985).
- ⁴⁷Hanyou Chu and Yia-Chung Chang, *Phys. Rev. B* **39**, 10861 (1989).
- ⁴⁸G. Oelgart, M. Proctor, D. Martin, F. Morier-Genoud, F.-K. Reinhart, B. Orschel, L. C. Andreani, and H. Rhan, *Phys. Rev. B* **49**, 10456 (1994).
- ⁴⁹G. D. Sanders and Yia-Chung Chang, *Phys. Rev. B* **32**, R5517 (1985).
- ⁵⁰U. Ekenberg and M. Altarelli, *Phys. Rev. B* **35**, 7585 (1987).
- ⁵¹H. Çelik, M. Cankurtaran, A. Bayrakli, E. Tiras, and N. Balkan, *Semicond. Sci. Technol.* **12**, 389 (1997).
- ⁵²S. Huant, A. Mandray, and B. Etienne, *Phys. Rev. B* **46**, 2613 (1992).
- ⁵³D. F. Nelson, R. C. Miller, and D. A. Kleinman, *Phys. Rev. B* **35**, R7770 (1987).
- ⁵⁴V. Ariel Altschul, A. Fraenkel, and E. Finkman, *J. Appl. Phys.* **71**, 4382 (1992).
- ⁵⁵H. Iwamura, H. Kobayashi, and H. Okamoto, *Jpn. J. Appl. Phys., Part 2* **23**, L795 (1984).
- ⁵⁶E. Grilli, M. Guzzi, R. Zamboni, and L. Pavesi, *Phys. Rev. B* **45**, 1638 (1992).
- ⁵⁷S. Rudin, T. L. Reinecke, and B. Segall, *Phys. Rev. B* **42**, 11218 (1990).
- ⁵⁸J. Christen and D. Bimberg, *Phys. Rev. B* **42**, 7213 (1990).
- ⁵⁹M. Colocci, M. Gurioli, and A. Vinattieri, *J. Appl. Phys.* **68**, 2809 (1990).
- ⁶⁰J. Humlíček, E. Schmidt, L. Bočánek, R. Švehla, and K. Ploog, *Phys. Rev. B* **48**, 5241 (1993).
- ⁶¹R. Kumar, S. S. Prabhu, and A. S. Vengurlekar, *Phys. Scr.* **56**, 308 (1997).
- ⁶²S. Rudin and T. L. Reinecke, *Phys. Rev. B* **66**, 085314 (2002).
- ⁶³A. Thränhardt, C. Ell, S. Mosor, G. Rupper, G. Khitrova, H. M. Gibbs, and S. W. Koch, *Phys. Rev. B* **68**, 035316 (2003).
- ⁶⁴H. Zhao, S. Wachter, and H. Kalt, *Phys. Rev. B* **66**, 085337 (2002).
- ⁶⁵A. Venu Gopal, R. Kumar, A. S. Vengurlekar, A. Bosacchi, S. Franchi, and L. N. Pfeiffer, *J. Appl. Phys.* **87**, 1858 (2000).
- ⁶⁶D. Gammon, S. Rudin, T. L. Reinecke, D. S. Katzer, and C. S. Kyono, *Phys. Rev. B* **51**, 16785 (1995).
- ⁶⁷It is deserving to consider briefly this criterion and screening issues comparing the 2D and 3D data. It is shown [G. Tränkle, H. Leier, A. Forchel, H. Haug, C. Ell, and G. Weimann, *Phys. Rev. Lett.* **58**, 419 (1987)] that the absolute values of the band-gap shifts in two dimensions are found to be much larger than the corresponding three-dimensional ones for equivalent electron-hole-plasma densities. However, in appropriate Rydberg units, the band-gap shift in the 2D case is considerably weaker than in the 3D case. The dimensionality dependence of the band-gap shift is traced to the different screening efficiencies in 3D and 2D systems. The latter effect was evidenced experimentally by demonstrating that excitons continue to dominate in the radiative recombination at doping levels right up to metallic limit [C. I. Harris, B. Monemar, H. Kalt, and K. Köhler, *Phys. Rev. B* **48**, 4687 (1993); P. O. Holtz, A. C. Ferreira, B. E. Sernelius, A. Buyanov, B. Monemar, O. Mauritz, U. Ekenberg, M. Sundaram, K. Campman, J. L. Merz, and A. C. Gossard, *ibid.* **58**, 4624 (1998)]. As concerns Mott criterion for the two-dimensional case, it has a form of product of square root of impurity density and Bohr radius to be equal to a certain constant [J. Kortus and M. Monecke, *Phys. Rev. B* **49**, 17216 (1994)]. If one assumes that the screening is not strongly QW width-dependent, critical impurity concentration needed for the Mott transition in QWs can depend not only on impurity types, but also on the quantum well width through the alteration of the impurity binding energy and Bohr radius.
- ⁶⁸J. Kundrotas, A. Čerškus, S. Ašmontas, A. Johannessen, G. Valušis, B. Sherliker, M. P. Halsall, P. Harrison, and M. J. Steer, *Lith. J. Phys.* **45**, 201 (2005). It is worth mentioning, also, that quite recently it was demonstrated experimentally [M. Carras, V. Berger, X. Marcadet, and B. Vinter, *Phys. Rev. B* **70**, 233310 (2004)] that the Mott transition in *n*-type-doped GaAs/Al_{0.3}Ga_{0.7}As $L_W=5$ nm MQW occur in the region 2×10^{11} and 4×10^{11} cm⁻² (equivalent in bulk material 10^{18} and 4×10^{18} cm⁻³), i.e., at higher doping concentration in comparison to that in a bulk *n*-type GaAs (2×10^{16} cm⁻³).
- ⁶⁹This adoption is based on the following considerations: Introduction of Be acceptors in GaAs/AlAs QW lifts the degeneracy of the valence band at the Γ point as the QW potential reduces the point group symmetry from T_d to D_{2d} [W. T. Masselink, Y. C. Chang, and H. Morkoç, *Phys. Rev. B* **28**, 7373 (1983); A. A. Reeder, B. D. McCombe, F. A. Chambers, and G. P. Devane,

- ibid.* **38**, 4318 (1988)]. As a result, the ground state $1S_{3/2}(\Gamma_8)$ of neutral acceptor Be splits into two doublets, namely, $1S_{3/2}(\Gamma_6)$ and $1S_{3/2}(\Gamma_7)$: A more strongly bound state of dominating heavy-hole character and another state associated mainly with the light-hole subbands. These states are strongly mixed and assignment to particular subbands, is in principle, only applicable for the excited acceptor states. Experimentally, in the PL spectra, only the lowest heavy-hole acceptor ground state plays an important role. The heavy-hole–light-hole splitting of the acceptor ground state in a QW can be resolved in photoluminescence excitation or selective photoluminescence spectra [P. O. Holtz, Q. X. Zhao, B. Monemar, M. Sundaram, J. L. Merz, and A. C. Gossard, *Phys. Rev. B* **47**, 15675 (1993)].
- ⁷⁰D. M. Eagles, *J. Phys. Chem. Solids* **16**, 76 (1960).
- ⁷¹W. P. Dumke, *Phys. Rev.* **132**, 1998 (1963).
- ⁷²H. Barry Bebb and E. W. Williams, in *Photoluminescence I: Theory, In Semiconductors and Semimetals*, edited by R. K. Willardson and A. C. Beer (Academic Press, New York, 1972), Vol. 8, p. 181.
- ⁷³P. Blood, *IEEE J. Quantum Electron.* **QE-36**, 354 (2000).
- ⁷⁴E. J. Johnson, in *Absorption Near the Fundamental Edge, In Semiconductors and Semimetals*, edited by R. K. Willardson and A. C. Beer (Academic Press, New York, 1967), Vol. 3, p. 153.
- ⁷⁵T. S. Moss, G. J. Burrell, and B. Ellis, *Semiconductor Optoelectronics* (Butterworth & Co. Publishers Ltd, London, 1973).
- ⁷⁶G. Bastard, *Phys. Rev. B* **24**, 4714 (1981).
- ⁷⁷R. C. Miller and A. C. Gossard, *Appl. Phys. Lett.* **43**, 954 (1983).
- ⁷⁸L. E. Oliveira and J. López-Gondar, *Phys. Rev. B* **41**, 3719 (1990).
- ⁷⁹M. H. Meynadier, J. A. Brum, C. Delalande, M. Voos, F. Alexandre, and J. L. Liévin, *J. Appl. Phys.* **58**, 4307 (1985).
- ⁸⁰D. C. Reynolds, K. G. Merkel, C. E. Stutz, K. R. Evans, K. K. Bajaj, and P. W. Yu, *Phys. Rev. B* **43**, 1604 (1991).
- ⁸¹D. J. Ashen, P. J. Dean, D. T. J. Hurle, J. B. Mullin, A. M. White, and P. D. Greene, *J. Phys. Chem. Solids* **36**, 1041 (1975).
- ⁸²C. B. Duke and G. D. Mahan, *Phys. Rev.* **139**, A1965 (1965).
- ⁸³J. D. Dow, D. L. Smith, and F. L. Lederman, *Phys. Rev. B* **8**, 4612 (1973).
- ⁸⁴G. T. Einevoll and Yia-Chung Chang, *Phys. Rev. B* **41**, 1447 (1990).
- ⁸⁵P. O. Holtz, Q. X. Zhao, A. C. Ferreira, B. Monemar, M. Sundaram, J. L. Merz, and A. C. Gossard, *Phys. Rev. B* **48**, 8872 (1993).
- ⁸⁶Q. Huang and R. G. Ulbrich, *J. Lumin.* **99**, 19 (2002).
- ⁸⁷J. Kundrotas, A. Čerškus, S. Ašmontas, G. Valušis, B. Sherliker, M.-P. Halsall, P. Harrison, and M.-J. Steer, *Acta Phys. Pol. A* **107**, 245 (2005).
- ⁸⁸M. Germain, E. Kartheuser, A. L. Gurskii, E. V. Lutsenko, I. P. Marko, V. N. Pavlovskii, G. P. Yablonskii, K. Heime, M. Heuken, and B. Schineller, *J. Appl. Phys.* **91**, 9827 (2002).
- ⁸⁹E. W. Williams and H. B. Bebb, *J. Phys. Chem. Solids* **30**, 1289 (1969).